

Optimal Scheduling of Electricity and Water in Renewable-Colocated Desalination Plants

Ahmed S. Alahmed*, Audun Botterud, Saurabh Amin, and Ali Al-Awami

Abstract—We develop a mathematical framework for the optimal scheduling of flexible water desalination plants (WDPs) as hybrid generator-load resources. WDPs integrate thermal generation, membrane-based controllable loads, and renewable energy sources, offering unique operational flexibility for power system operations. They can simultaneously participate in two markets: selling desalinated water to a water utility, and bidirectionally transacting electricity with the grid based on their net electricity demand. We formulate the scheduling decision problem of a profit-maximizing WDP, capturing operational, technological, and market-based coupling between water and electricity flows. The threshold-based structure we derive provides computationally tractable coordination suitable for large-scale deployment, offering operational insights into how thermal generation and membrane-based loads complementarily provide continuous bidirectional flexibility. The thresholds are analytically characterized in closed form as explicit functions of technology and tariff parameters. We examine how small changes in the exogenous tariff and technology parameters affect the WDP’s profit. Extensive simulations illustrate the optimal WDP’s operation, profit, and water-electricity exchange, demonstrating significant improvements relative to benchmark algorithms.

Index Terms—Desalination, optimal scheduling, renewable energy, reverse-osmosis, threshold policies, water-power systems.

I. INTRODUCTION

THE ongoing transformation of power systems, driven by increasing penetration of variable renewables, creates growing demand for flexible resources that can provide bidirectional grid services. Water desalination plants (WDPs),¹ representing approximately 5-12% of total electricity consumption in Middle East countries [3] with 7% per annum global capacity growth since 2010 [4], are evolving from passive to active market participants capable of dynamically adjusting operations in response to price signals and renewable energy availability. Unlike conventional generators that can only supply power or loads that can only reduce consumption, modern WDPs integrating both thermal and renewable generation and membrane-based loads function as hybrid generator-load resources with continuous bidirectional flexibility.

With global freshwater demand projected to exceed available supply by 40% by 2030 [5], WDPs have become an increasingly vital component of sustainable water infrastructure in various parts of the world. As the demand for seawater and wastewater treatment continues to grow, so does the need for efficient and sustainable operation of WDPs. These facilities are inherently energy-intensive, consuming substantial

¹By WDP, we also refer to water treatment plants. The two differ only in terms of the salinity coefficients considered [2].

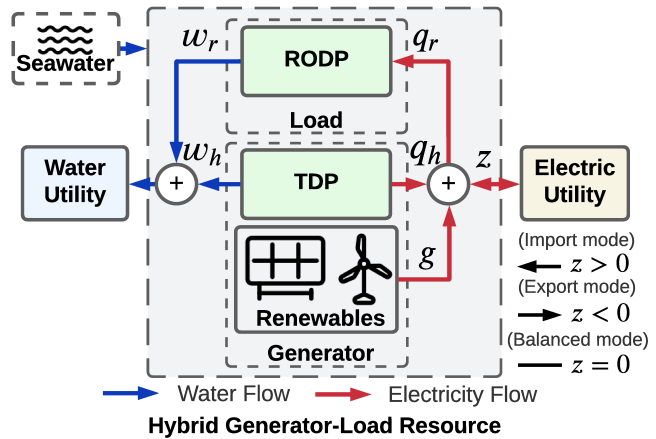


Fig. 1. WDP as a hybrid generator-load resource. The water (power) output of the thermal desalination plant (TDP) and reverse osmosis desalination plant (RODP) is denoted by w_h, w_r ($q_h, q_r \in \mathbb{R}_+$, respectively). The renewable generation and net consumption are denoted by $g \in \mathbb{R}_+$, and $z \in \mathbb{R}$.

amounts of energy to drive both thermal- and membrane-based desalination processes [6]. Consequently, there is growing interest in integrating desalination operations with renewable energy sources and advanced scheduling strategies to reduce operational costs and environmental impact [7].

In parallel, the ongoing transformation of power systems, driven by increasing penetration of renewables and the rise of decentralized energy resources, has given rise to novel opportunities and challenges at the water-energy nexus. In this context, WDPs are evolving from passive energy consumers to active participants in electricity markets, capable of dynamically adjusting their operations in response to electricity price signals and renewable energy availability. Co-optimizing water and power scheduling, a global research priority in the water-energy nexus [8], is crucial for ensuring economic viability and grid-supportive behavior.

This paper develops an analytical framework for the optimal scheduling of WDPs operating as hybrid generator-load resources (Fig.1). A key challenge lies in utilizing the complementarities between the load-generator resources within the plant, in addition to optimally scheduling both water and electricity transactions with water and electric utilities.

A. Related Work

One of the earliest examinations of water-power systems is Gleick’s seminal review [9], which highlighted the fundamental interdependence between water and power systems: energy is required for water extraction, treatment, and transport, while water is essential for electricity generation and fuel production.

This foundational perspective has since motivated a broad literature on modeling, coordinating, and optimizing coupled water-energy infrastructures.

In energy-abundant regions, TDPs often operate alongside power generation, producing freshwater as the primary output and electricity as a by-product. These colocated systems leverage shared thermal and electrical infrastructure, resulting in strongly coupled operational behavior. For instance, [10] propose dynamic, physics-based models of such integrated systems, emphasizing the value of coordinated control between thermal power and thermal desalination units.

Reverse osmosis (RO) has emerged as the dominant desalination technology, favored for its modularity and superior energy efficiency. Recent estimates suggest that RO accounts for approximately 69% of global installed desalination capacity [4]. As RO units rely predominantly on electricity from the grid, they can function as substantial and flexible loads within the power system. Several recent studies [11]–[14] explore the integration of RODPs with variable renewable energy sources (e.g., solar and wind), primarily through simulation-based energy management frameworks designed to reduce operational costs, emissions, and improve grid compatibility. In particular, [14] present an energy management system for a standalone wind-powered desalination microgrid, highlighting coordinated control strategies for matching variable generation to water demand. However, these contributions remain largely simulation-based and typically treat the power system as an exogenous input, without explicitly modeling the endogenous coupling between the water and energy sectors. More recent efforts [15]–[17] address this gap by developing numerical co-optimization models for water-energy microgrids and joint RO-power dispatching under dynamic demand, grid constraints. These studies also explore the role of RO in demand response and grid services. The work in [18] formulates a security-constrained unit commitment problem to coordinate the operation of RO-only desalination plants and power plants and showed a reduction in the system's operating costs by 5% to 8% under the IEEE 118-bus system.

Despite these advances, existing approaches are predominantly computational, with limited analytical insight into structural properties of the optimal scheduling problem, an issue that our work aims to address.

Beyond RO-power coordination, recent work expands to decentralized water-energy nexus markets and flexible cross-sector operations. [19] propose a blockchain-based transactive framework for interconnected water-energy hubs, showing performance gains under spatial-temporal uncertainty. Similarly, [20] develops a watershed-electricity model that exploits hydrological flexibility, through dynamic river conditions and pump scheduling, to support distribution network operations. While demonstrating the benefits of decentralized coordination, these studies do not consider colocating and the unique operating regimes of joint RO and TDP systems.

The studies in [2], [21], [22] propose models for coordinating water and power distribution systems to minimize operational costs of meeting water and electricity demands by leveraging variable speed pumps and water tanks. However, these models do not incorporate colocated renewable energy

sources or bidirectional energy transactions between WDPs and the electric grid, limiting their ability to fully optimize integrated resource management.

Although significant progress has been made, most existing work models RODP and TDP separately, without capturing their distinct operational features or interactions with water and power systems, particularly when colocated with renewables. This siloed treatment overlooks opportunities for coordinated real-time scheduling and efficient resource utilization. In addition, existing studies are predominantly numerical- and simulation-based, whereas we develop an analytical framework that enables scalable solutions with structural insights, including operational intuitions and comparative statics.

B. Main Contributions

Our main contribution is the analytical characterization of the optimal electricity-water scheduling for WDPs operating as hybrid generator-load resources, enabling efficient grid integration while maintaining water production requirements. The threshold-based structure we derive provides computationally tractable coordination suitable for large-scale deployment, offering operational insights into how thermal generation and membrane-based loads complementarily provide continuous bidirectional flexibility.

From a power system operations perspective, our results demonstrate how WDPs can provide: (i) bidirectional dispatch flexibility (import, balanced, export modes) without energy storage; (ii) combined response from coordinated generation-load control; (iii) predictable dispatch through thresholds computable offline and independent of renewables; (iv) smooth zero-crossing transitions valuable for renewable integration.

Fig.2 shows the WDP's optimal water dispatch, also determining power dispatch, based on renewable generation (g), effective RODP water price ($f'_r \pi^w$), and grid prices of imports (π^+) and exports (π^-). The WDP's operation is segmented into three modes (IM, NZ, EX) depending on renewables output by two thresholds (Γ_{IM}, Γ_{EX}). It operates as a controllable load in the (IM) mode, a net-zero self-sufficient microgrid in the (NZ) mode, and a dispatchable generator in the (EX) mode.

As illustrated in Fig.2, the TDP's optimal water and power outputs decrease monotonically with the availability of local renewables, whereas the RODP's water output increases monotonically with renewables. If the marginal value of electricity when water is produced via the RODP $f'_r \pi^w$ exceeds π^+ , the RODP operates at its maximum capacity, as the marginal revenue from water sales surpasses the marginal cost of power, thereby expanding the (IM) mode. Conversely, if $f'_r \pi^w < \pi^-$, the RODP is scheduled at its minimum capacity, expanding the (EX) mode. In both boundary cases, *i.e.*, when $f'_r \pi^w \notin [\pi^-, \pi^+]$, TDP output adjusts to renewable availability according to a two-threshold policy. In the power-balanced, net-zero (NZ) mode, the TDP generation follows the renewable-adjusted RODP consumption.

The most pertinent scenario arises when the marginal value of electricity when water is produced via RO exceeds the power export price but remains below the import price, *i.e.*, $f'_r \pi^w \in [\pi^-, \pi^+]$. Under this condition, we demonstrate that

the optimal schedules for TDP and RODP exhibits four-threshold and two-threshold structures, respectively. As onsite renewables increase, both TDP and RODP dynamically adjust to absorb surplus generation, expanding the power-balanced (NZ) mode while shrinking the power-importing (IM) and exporting (EX) modes.

In addition to the general structure of the solution, we analyze the optimal WDP dispatch in cases of single desalination technology. Also, we show the effect of the exogenous water and electricity tariff and technology parameters on the WDP's maximum profit. We provide extended simulation results illustrating the optimal WDP's profit, scheduling, and patterns of water and electricity exchange compared to benchmarks.

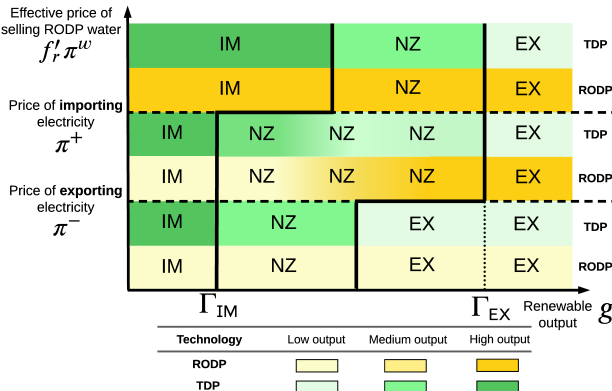


Fig. 2. Optimal WDP water dispatch across electricity operating modes (IM: import, NZ: net-zero, EX: export).

C. Major Mathematical Symbols and Paper Organization

Table I lists the major symbols and notations used. The WDP system model and scheduling problem are presented in §II, followed by a delineation of the optimal scheduling and its intuitions in §III. Analysis on special cases and comparative statics of the optimal scheduling policy is provided in §IV. Detailed simulations are shown in §V, followed by the conclusion and directions for future research in §VI.

II. WDP FRAMEWORK AND DISPATCH PROBLEM

From a grid operator perspective, the WDP represents a controllable hybrid resource capable of both generation and consumption. Unlike conventional resources with unidirectional power flow, the WDP can smoothly transition between grid import, balanced, and export states through coordinated control of TDP and RODP units. This section formalizes the WDP's operational characteristics and scheduling problem.

We consider the problem of a WDP that jointly optimizes water and electricity schedules to maximize its profits from transacting the two commodities with water and electric utilities (Fig.1). The WDP integrates thermal and membrane-based desalination units, colocated with renewables on-site. It engages in a unilateral transaction with the water utility, whereby it supplies water at an exogenously specified price, which may vary over time. In contrast, its interaction with the electricity utility is bilateral: the WDP purchases electric power when its demand exceeds local generation and exports

TABLE I
WDP MAJOR VARIABLES AND PARAMETERS

Symbol	Description
Decision and Exogenous Variables	
g	Renewable DG output.
q_h, q_r	Electricity production (consumption) of TDP (RODP).
w_h, w_r	Water output of TDP and RODP.
w_h^*, w_r^*	Optimal water output of TDP and RODP.
z	Net electricity exchange.
Technical Parameters and Functions	
α_h	TDP fuel-to-water conversion factor.
α_r	RODP electricity-to-water conversion factor.
β_h	TDP fuel-to-electricity conversion factor.
η_h	TDP water-to-electricity production ratio.
$f_h(\cdot), f_r(\cdot)$	Conversion functions of TDP and RODP.
$\underline{w}_h, \overline{w}_h$	Minimum and maximum water flowrates of TDP.
$\underline{w}_r, \overline{w}_r$	Minimum and maximum water flowrates of RODP.
Γ_{IM}, Γ_{EX}	Mode-defining optimal scheduling thresholds.
$\Gamma_{NZ_1}, \Gamma_{NZ_2}$	Internal optimal scheduling thresholds.
Prices, Costs, and Profit	
$C_h(\cdot), C'_h(\cdot)$	TDP cost function and its derivative.
p_h	TDP fuel consumption.
$\Pi(\cdot)$	WDP profit function.
$P(\cdot)$	Electricity payment function.
π^+, π^-	Electricity retail (import) and sell (export) prices.
π^w	Water selling price.
$R^w(\cdot)$	Water revenue function.
Mathematical Notations	
\mathbb{R}_+	Set of nonnegative real numbers, <i>i.e.</i> , $\{x \in \mathbb{R} \mid x \geq 0\}$
\mathbb{R}_{++}	Set of positive real numbers, <i>i.e.</i> , $\{x \in \mathbb{R} \mid x > 0\}$
$[x]^+$	$\max\{0, x\}$, for any $x \in \mathbb{R}$
$[x]^-$	$-\min\{0, x\}$, for any $x \in \mathbb{R}$
$[x]_{[a,b]}$	$\max\{a, \min\{x, b\}\}$, with $x, a, b \in \mathbb{R}$ and $a \leq b$

surplus power otherwise. This arrangement is structurally analogous to virtual power plants [23] and grid-connected microgrids [24]. In both the water and electricity markets, the WDP is modeled as a price-taking agent, with its dispatch affecting quantities but not market-clearing prices.

As shown in Figures 1 and 2, the WDP exhibits a noteworthy complementarity between water and electricity systems. Specifically, the TDP uses a fuel source to co-generate both water and electricity, while the RODP consumes electricity to produce water. As a result, the electrical load within the WDP is the RODP, whose demand is met through a combination of local generation from the TDP, on-site renewables, and electricity imported from the grid, with contributions varying based on availability and operating conditions.

The WDP's operational timescale is set by its measurement and scheduling frequency, while transactions with water and electric utilities follow their billing periods (e.g., 15 min or hourly). To streamline the exposition, we assume the WDP's scheduling period matches the utilities' billing period, allowing a single time-step formulation.

Next, we present the modeling of the TDP, RODP, payment functions to the water and electricity utilities, and the WDP scheduling problem.

A. WDP Resources

1) *TDP*: TDPs use a boiler to heat seawater using a fuel source,² producing steam that is then condensed to obtain fresh water. The waste heat is sourced to power a turbine to produce electricity. TDPs, therefore, produce both water and electricity.

The TDP, therefore, consumes fuel, denoted by p_h , and produces both water and electricity, which we denote by $w_h \in \mathbb{R}_+$ and $q_h \in \mathbb{R}_+$, respectively. We adopt a standard linear function of TDP desalinated water $w_h = f_h(p_h) = \alpha_h p_h$, where $\alpha_h \in \mathbb{R}_+$ is the thermal conversion factor (m³/BTU) that represents the consumed fuel (BTU) for each cubic meter of desalinated water (m³) [25]. We use f'_h to denote the derivative of f_h with respect to p_h , *i.e.*, $f'_h := \frac{\partial f_h(p_h)}{\partial p_h}$.

The TDP generates electricity as a by-product of water desalination according to the relation $w_h = \eta_h q_h$, where $\eta_h \in \mathbb{R}_+$ is the water-to-electricity production ratio (m³/kW) [10]. Define $\beta_h := \alpha_h / \eta_h \in \mathbb{R}_+$, which is the thermal conversion factor (kW/BTU) from fuel to electricity.

The TDP water flowrate is bounded by the maximum $\bar{w}_h \in \mathbb{R}_+$ and minimum $\underline{w}_h \in \mathbb{R}_+$ operating limits that ensure stable operation, *i.e.*, $w_h \in [\underline{w}_h, \bar{w}_h]$.

The TDP's operating cost function is denoted by $C_h(p_h) \in \mathbb{R}$, which depends on the fuel cost and plant efficiency. We assume the cost function $C_h(\cdot)$ to be strictly convex, continuously differentiable, and non-decreasing. Define $C'_h := \frac{\partial C_h(p_h)}{\partial p_h}$ and $D_h(\cdot)$ as the inverse of $C'_h(\cdot)$.

2) *RODP*: The RODP consumes electricity to force pressure seawater (or wastewater) molecules through a semi-permeable membrane under high pressure, effectively filtering out salt and impurities [26].

The water production and electricity consumption of the RODP, $w_r, q_r \in \mathbb{R}_+$, respectively, are related as $w_r = f_r(q_r) = \alpha_r q_r$, where $\alpha_r \in \mathbb{R}_+$ is the RODP's conversion factor. We use f'_r to denote the derivative of f_r with respect to q_r , *i.e.*, $f'_r := \frac{\partial f_r(q_r)}{\partial q_r}$.

The water production of the RODP is bounded from above by the maximum $\bar{w}_r \in \mathbb{R}_+$ flowrate and from below by the minimum $\underline{w}_r \in \mathbb{R}_+$ operating limits, *i.e.*, $w_r \in [\underline{w}_r, \bar{w}_r]$.

3) *Renewable Energy Sources*: The plant has local renewables whose aggregate generation is denoted by $g \in \mathbb{R}_+$. We assume perfect forecasts of renewable generation. This is a simplifying assumption supported by the smoothing effect of coupling renewables with energy storage and the increasing accuracy of machine learning-based forecasting methods [27], [28]. Capital costs of renewable installations are excluded from the analysis, as we focus on short-run operational dispatching rather than long-term capacity planning.

B. WDP Water and Electricity Payments

1) *Water Revenue*: The profit-maximizing WDP sells the total desalinated water from the TDP and RODP to a water utility; therefore, the WDP revenue function is given by

$$R^w(w_h, w_r) = \pi^w(w_h + w_r), \quad (1)$$

where $\pi^w \in \mathbb{R}_+$ is the water selling price.

²Fuel sources may include fossil-based (e.g., natural gas, oil), nuclear, hydrogen-based, or other energy sources, depending on the system's design and regional energy availability.

2) *Electricity Payment*: The profit-maximizing WDP transacts with the electric utility, which charges the WDP based on its net electricity exchange function $z : \mathbb{R}_+ \times \mathbb{R}_+ \rightarrow \mathbb{R}$, given by

$$z(q_r, q_h; g) = q_r - q_h - g. \quad (2)$$

The electric utility charges the WDP as an industrial customer under a net energy metering tariff, as

$$P(q_r, q_h; g) = \pi^+[z(q_r, q_h; g)]^+ - \pi^-[z(q_r, q_h; g)]^- + \pi^0, \quad (3)$$

where the parameters $(\pi^+, \pi^-) \in \mathbb{R}_+$ represent the import and export prices, respectively, and $\pi^0 \in \mathbb{R}$ the non-volumetric fixed charge. To avoid utility death spirals and risk-free arbitrage by the WDP, we assume $\pi^+ \geq \pi^-$. A special case of (3) is when the WDP faces a single price ($\pi^+ = \pi^-$), *e.g.*, an WDP facing LMPs as in competitive electricity markets. From (3), the WDP is a *power-importer* (IM) if $z > 0$, *power-exporter* (EX) if $z < 0$, and *power-balanced* (NZ) if $z = 0$.

Under a multi-interval formulation, water and electricity payments naturally generalize to time-varying prices, such as time-of-use or real-time tariffs, which may be updated monthly or seasonally [29]. Alternatively, utilities can establish long-term contracts with desalination plants that fix import and export prices.

C. WDP Profit

The profit function of the WDP is given by

$$\Pi(w_h, w_r, q_h, q_r; g) := R^w(w_h, w_r) - P(q_r, q_h; g) - C_h(p_h), \quad (4)$$

where the first term represents the revenue from water sales; the second represents the monetary transaction from net electricity consumption, which constitutes a cost when electricity is imported, and a revenue when it is exported; and the third term reflects the operating costs of the TDP. In contrast, RODP operating costs are implicitly accounted for through the cost of procuring energy q_r , which can be sourced from colocated renewables, TDP, grid, or any combination thereof.

D. Profit-Maximizing WDP Dispatch

The WDP jointly schedules thermal and RO units to maximize profit under capacity and energy balance constraints; hence, it solves

$$\begin{aligned} (w_h^*, w_r^*, q_h^*, q_r^*) := & \underset{w_h, q_h, w_r, q_r \in \mathbb{R}_+}{\operatorname{argmax}} \Pi(w_h, w_r, q_h, q_r; g) \\ \text{subject to } & z = q_r - q_h - g \\ & w_h + w_r \geq \mathcal{W} \\ & \underline{w}_h \leq w_h \leq \bar{w}_h \\ & \underline{w}_r \leq w_r \leq \bar{w}_r, \end{aligned} \quad (5)$$

where $\mathcal{W} \in \mathbb{R}_+$ is the total demand of desalinated water. We assume that the WDP is sized so that the minimum output of desalinated water is no less than that demanded by the water utility, *i.e.*, $\underline{w}_h + \underline{w}_r \geq \mathcal{W}$. The scheduling problem in (5) is well-posed with global optima, as the objective is concave (Lemma 1) over a convex and closed set.

Lemma 1 (Concavity of $\Pi(\cdot)$). *Given $\pi^+ \geq \pi^-$, the profit function $\Pi(\cdot)$ is strictly concave in w_h and concave in w_r .*

Proof. See the Appendix. \square

Although the problem is concave, the objective function is non-differentiable due to the presence of indicator functions in the electricity payment expression in (3).

III. OPTIMAL WDP DISPATCH

This section characterizes the optimal WDP dispatch, which jointly optimizes water and electricity production and consumption, and highlights its structural properties. §III-A–III-C delineate the structure of the optimal WDP dispatch when $f'_r \pi^w \in [\pi^-, \pi^+]$. The cases where $f'_r \pi^w \notin [\pi^-, \pi^+]$ are less involved and addressed separately in Proposition 2 in §III-D.

A. Optimal WDP Dispatch Policy

The optimal joint dispatch of the TDP and RODP obeys a threshold structure that dictates the plants' optimal setpoints based on the renewables g , as shown in Theorem 1.

Theorem 1 (Optimal WDP dispatch). *Given g , and when $f'_r \pi^w \in [\pi^-, \pi^+]$, the optimal TDP and RODP water dispatch obey a four-threshold and two-threshold policies, respectively. The thresholds $\Gamma_{\text{IM}}, \Gamma_{\text{NZ}_1}, \Gamma_{\text{NZ}_2}, \Gamma_{\text{EX}} \in \mathbb{R}$ are given by*

$$\begin{aligned} \Gamma_{\text{IM}} &:= \underline{w}_r / f'_r - w_h^{\text{IM}} / \eta_h, & \Gamma_{\text{NZ}_1} &:= \underline{w}_r / f'_r - w_h^{\text{NZ}} / \eta_h, \\ \Gamma_{\text{NZ}_2} &:= \bar{w}_r / f'_r - w_h^{\text{NZ}} / \eta_h, & \Gamma_{\text{EX}} &:= \bar{w}_r / f'_r - w_h^{\text{EX}} / \eta_h, \end{aligned} \quad (6)$$

where, for $\sigma \in \{\text{IM}, \text{NZ}, \text{EX}\}$,

$$w_h^\sigma := [f'_h D_h (f'_h \pi^w + \beta_h \delta^\sigma)]_{[\underline{w}_h, \bar{w}_h]} \quad (7)$$

and $\delta^{\text{IM}} := \pi^+$, $\delta^{\text{NZ}} := f'_r \pi^w$, $\delta^{\text{EX}} := \pi^-$.

Given g and the thresholds, the optimal TDP and RODP setpoints are, respectively, given by

$$w_h^*(g) = \begin{cases} w_h^{\text{IM}} & , g < \Gamma_{\text{IM}} \\ [\eta_h (\underline{w}_r / f'_r - g)]_{[\underline{w}_h, \bar{w}_h]} & , g \in [\Gamma_{\text{IM}}, \Gamma_{\text{NZ}_1}] \\ w_h^{\text{NZ}} & , g \in [\Gamma_{\text{NZ}_1}, \Gamma_{\text{NZ}_2}] \\ [\eta_h (\bar{w}_r / f'_r - g)]_{[\underline{w}_h, \bar{w}_h]} & , g \in (\Gamma_{\text{NZ}_2}, \Gamma_{\text{EX}}] \\ w_h^{\text{EX}} & , g > \Gamma_{\text{EX}}, \end{cases} \quad (8)$$

$$w_r^*(g) = \begin{cases} \underline{w}_r & , g < \Gamma_{\text{NZ}_1} \\ f'_r (w_h^{\text{NZ}} / \eta_h + g) & , g \in [\Gamma_{\text{NZ}_1}, \Gamma_{\text{NZ}_2}] \\ \bar{w}_r & , g > \Gamma_{\text{NZ}_2}. \end{cases} \quad (9)$$

Proof. See the Appendix. \square

Theorem 1 establishes that the WDP schedules the TDP and RODP by measuring renewable power generation and comparing it against four thresholds defined in (6), as illustrated in Figure 3. The following corollary formalizes the relationship among these thresholds.

Corollary 1 (Thresholds relationship). *The four thresholds defined in Theorem 1 satisfy the strict ordering $\Gamma_{\text{EX}} \geq \Gamma_{\text{NZ}_2} \geq \Gamma_{\text{NZ}_1} \geq \Gamma_{\text{IM}}$. Moreover, the gap between the outermost*

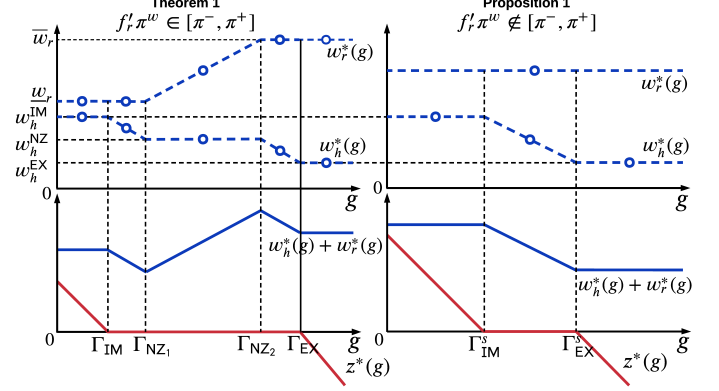


Fig. 3. Depiction of the optimal WDP dispatch in Theorem 1, i.e., when $f'_r \pi^w \in [\pi^-, \pi^+]$, and Proposition 2, i.e., when $f'_r \pi^w \notin [\pi^-, \pi^+]$. Top row: Optimal TDP and RODP water dispatch (when $w_h^{\text{IM}} < \bar{w}_r$) versus renewable generation. Bottom row: WDP's water and power transactions with the water and electric utilities versus renewable generation.

thresholds, $\Gamma_{\text{EX}} - \Gamma_{\text{IM}}$, increases monotonically with both the price differential $\Delta\pi := \pi^+ - \pi^-$ and the RODP flexibility range $\bar{w}_r - \underline{w}_r$.

Proof. See the Appendix. \square

Although Theorem 1 specifies only optimal water dispatch, it also implicitly schedules electricity consumption and production, given the RODP conversion function $f_r(\cdot)$ and the TDP water-to-power production ratio η_h .

The next proposition follows from Theorem 1, and it establishes the relation between the optimal threshold-based WDP dispatch and its bidirectional transaction with the grid.

Proposition 1 (Optimal grid exchange). *The thresholds $(\Gamma_{\text{IM}}, \Gamma_{\text{EX}})$ in Theorem 1 define the net-import mode of the WDP with respect to the electric utility, i.e.,*

$$z^*(g) \mapsto \text{sgn}(z^*(g)) = \begin{cases} 1 & , g < \Gamma_{\text{IM}} \\ 0 & , g \in [\Gamma_{\text{IM}}, \Gamma_{\text{EX}}] \\ -1 & , g > \Gamma_{\text{EX}}, \end{cases} \quad (10)$$

where $\text{sgn} : \mathbb{R} \rightarrow \{-1, 0, 1\}$.

Proof. See the Appendix. \square

Proposition 1 characterizes the WDP's value as a flexible grid resource. The thresholds $(\Gamma_{\text{IM}}, \Gamma_{\text{EX}})$ define three distinct grid-interaction modes, with the facility providing:

- Controllable load (IM): Net import $z^*(g) > 0$ with demand response capability.
- self-sufficient microgrid (NZ): Self-sufficient operation absorbing renewable variability (see the red curve in Figure 3).
- Dispatchable generator (EX): Net export $z^* < 0$ with controllable output.

Critically, transitions between modes occur continuously through internal balancing of generation (TDP and renewables) and load (RODP), avoiding the discrete switching characteristic of conventional resources. The zero-crossing flexibility is particularly valuable for renewable integration, as the WDP can smoothly absorb forecast errors without mode changes.

B. Optimal Dispatch Properties

We summarize five key structural properties of the optimal dispatch of the WDP, as characterized in Theorem 1.

- Renewable-independent thresholds: The optimal dispatch is governed by the four thresholds in (6) that depend only on water and electricity tariff parameters and conversion factors of the TDP and RODP and are computed *offline*, independent of renewables output g . The thresholds in (6) can be negative. Indeed, if $\bar{w}_r/f'_r \leq w_h^{\text{EX}}/\eta_h$, then $\Gamma_{\text{EX}} \leq 0$, and the WDP always operates in the net-export mode, because $g \geq 0$. Physically, this means that the TDP-generated power always exceeds RODP consumption.
- Monotonic and piecewise-linear dispatch: The optimal TDP output decreases monotonically with g , while the RODP output increases monotonically. Both follow a piecewise-linear profile segmented by the thresholds Γ_{NZ_1} and Γ_{NZ_2} for RODP and by all four thresholds for TDP. RODP water output is constant when $g \notin [\Gamma_{\text{NZ}_1}, \Gamma_{\text{NZ}_2}]$, and linear otherwise. The TDP output is constant everywhere except when $g \in [\Gamma_{\text{IM}}, \Gamma_{\text{NZ}_1}) \cup (\Gamma_{\text{NZ}_2}, \Gamma_{\text{EX}}]$.
- Closed-form characterization: The optimal setpoints $w_h^*(g), w_r^*(g)$ admit explicit closed-form expressions.
- Operational interdependence: In the net-zero mode, the TDP and RODP interchangeably use the increasing renewables to maintain energy-balancedness.
- RODP grid independence: The RODP dispatch is independent of the electricity import and export prices π^+ and π^- .

C. Operational Insights and Intuitions

In the sequel, we highlight some operational insights from the optimal WDP dispatch, which is depicted in Fig.3.

1) *RODP Optimal Dispatch*: Although the RODP variables are linear in the objective of (5), the RODP operates at its bounds only when $g \notin [\Gamma_{\text{NZ}_1}, \Gamma_{\text{NZ}_2}]$. When renewable output is low ($g < \Gamma_{\text{IM}}$), the WDP is a net importer ($z^*(g) > 0$) facing π^+ . Since $f'_r\pi^w < \pi^+$, the marginal revenue of RODP water is below the marginal cost of importing power, so the RODP is set to its minimum. Conversely, when renewables are high ($g > \Gamma_{\text{EX}}$) and the WDP is a net exporter ($z^*(g) < 0$) facing π^- , the RODP is set to maximum because $f'_r\pi^w \geq \pi^-$, *i.e.*, selling RODP water yields more value than exporting power.

The off-grid mode $g \in [\Gamma_{\text{IM}}, \Gamma_{\text{EX}}]$ is the more nuanced. Here, the WDP neither buys nor sells electricity, so revenue arises solely from water sales; thus, the marginal cost of TDP production governs dispatch. At $g = \Gamma_{\text{IM}}$, local generation (renewables and TDP) just meets RODP demand, and as g increases beyond Γ_{NZ_1} , renewables progressively displace TDP generation to reduce costs.

Because the TDP cost is convex with increasing marginal cost, for $g \in [\Gamma_{\text{IM}}, \Gamma_{\text{NZ}_1}]$ the marginal cost reduction from lowering TDP output exceeds the marginal revenue from increasing RODP output. Thus, RODP output stays fixed while the TDP adjusts to enforce the off-grid condition, and the share of renewables serving the RODP increases with g .

At $g = \Gamma_{\text{NZ}_1}$, the TDP marginal cost equals the marginal revenue of RODP water, so any additional renewables are used to increase RODP output. For $g \in [\Gamma_{\text{NZ}_1}, \Gamma_{\text{NZ}_2}]$, RODP

consumption increases as the TDP correspondingly decreases. At $g = \Gamma_{\text{NZ}_2}$, the RODP reaches its upper limit. Beyond this point, the WDP must export surplus renewables at value π^- or reduce the TDP output, whichever yields higher revenue; for $g \leq \Gamma_{\text{EX}}$, reducing the TDP output is preferred. When $g > \Gamma_{\text{EX}}$, the RODP is saturated, and the TDP marginal cost falls below π^- , so exporting becomes optimal.

2) *TDP Optimal Dispatch*: The TDP operates as a dual-output generator, producing water and power according to the combined marginal values of water $f'_h\pi^w$ and electricity $\beta_h\delta^\sigma$. TDP water is always valued at $f'_h\pi^w$. In the net-import mode, TDP power offsets grid imports and hence valued at $\beta_h\pi^+$, so TDP output depends on the sum $f'_h\pi^w + \beta_h\pi^+$ as in ((7)). Similarly, for net-export mode, the output depends $f'_h\pi^w + \beta_h\pi^-$. In the off-grid mode, TDP power is consumed locally by the RODP. Its effective value becomes $\eta_h f'_r\pi^w$, the marginal value of RODP water produced using TDP power. Thus, the TDP operates according to $(f'_h + f'_r\beta_h)\pi^w$.

D. Special Tariff Cases

Proposition 2 (Optimal dispatch under special tariff cases). *When $f'_r\pi^w \notin [\pi^-, \pi^+]$, the optimal RODP water output, for all g , is*

$$w_r^* = \begin{cases} \bar{w}_r & , f'_r\pi^w > \pi^+ \geq \pi^- \\ \underline{w}_r & , \pi^+ \geq \pi^- > f'_r\pi^w, \end{cases} \quad (11)$$

and, given g , the optimal TDP water dispatch becomes a two-threshold $(\Gamma_{\text{IM}}^s, \Gamma_{\text{EX}}^s)$ policy with

$$w_h^*(g) = \begin{cases} w_h^{\text{IM}} & , g < \Gamma_{\text{IM}}^s \\ [\eta_h(w_r^*/f'_r - g)]_{[\underline{w}_r, \bar{w}_r]} & , g \in [\Gamma_{\text{IM}}^s, \Gamma_{\text{EX}}^s] \\ w_h^{\text{EX}} & , g > \Gamma_{\text{EX}}^s, \end{cases} \quad (12)$$

where $\Gamma_{\sigma}^s = w_r^*/f'_r - w_h^{\sigma}/\eta_h$.

When $\pi^+ = \pi^-$, the optimal RODP water output is as in (11), and the optimal TDP water output is $w_h^* = w_h^{\text{IM}}$.

Proof. See the Appendix. \square

Proposition 2 is depicted in Fig.3. When $f'_r\pi^w > \pi^+ \geq \pi^-$, the revenue from selling water is higher than the cost of importing power, hence the RODP is always at maximum. Conversely, when $f'_r\pi^w < \pi^- \leq \pi^+$, selling power is worth more than selling water, hence the RODP is set to a minimum. In both cases, TDP dispatch and net electricity exchange with the grid are governed by two thresholds that partition the renewables' range into the three modes (IM, NZ, EX).

IV. SPECIAL CASES AND MAXIMUM PROFITS

We discuss in §IV-A a special case arising from the WDP's available desalination technology, and in §IV-B the WDP's profits under optimal dispatch decisions.

A. Special Technology Cases: RODP-Only and TDP-Only

We formalize, in Corollary 2, the WDP's optimal dispatch when only a single desalination technology is available, *i.e.*, either an RODP or TDP.

Corollary 2 (Optimal dispatch under single desalination technology). *For an RODP-only WDP, the optimal dispatch is a two-threshold policy, given by*

$$w_r^*(g) = \begin{cases} \underline{w}_r & , g < \underline{w}_r/f'_r \\ f'_r g & , g \in [\underline{w}_r/f'_r, \bar{w}_r/f'_r] \\ \bar{w}_r & , g > \bar{w}_r/f'_r. \end{cases} \quad (13)$$

For a TDP-only WDP, the optimal dispatch is $w_h^* = w_h^{\text{EX}}$.

Proof. See the Appendix. \square

In the RODP-only case, the WDP behaves as a controllable load under net metering, arbitraging import and export prices [29]. Whereas, in the TDP-only case, the WDP is always a producer of both water and power. Consequently, the optimal operating point, being price dependent, remains constant.

B. WDP Profits under Optimal Dispatch

Here, we formalize that the WDP profit under optimal dispatch decisions is monotonically increasing with g with a decreasing derivative. We also show how small changes in the exogenous parameters $(\pi^+, \pi^-, \pi^w, \alpha_r, \alpha_h, \beta_h)$ affect the WDP's optimal dispatch and profits.

Theorem 2 (Operation profit sensitivity analysis). *The WDP maximum profit increases monotonically with renewable generation at the rate of π^+ when $g < \Gamma_{\text{IM}}$, $f'_r \pi^w$ when $g \in [\Gamma_{\text{NZ}_1}, \Gamma_{\text{NZ}_2}]$, and π^- when $g > \Gamma_{\text{EX}}$. When $g \in [\Gamma_{\text{IM}}, \Gamma_{\text{NZ}_1})$ the profit increases at rates $x \in [\pi^+, f'_r \pi^w]$, while when $g \in (\Gamma_{\text{NZ}_2}, \Gamma_{\text{EX}}]$ the profit increases at rates $x \in [f'_r \pi^w, \pi^-]$.*

Moreover, the WDP maximum profit is (i) decreasing in the electricity import price π^+ , (ii) increasing in the electricity export price π^- , (iii) increasing in the water price π^w , and (iv) increasing in the RODP energy-to-water conversion factor α_r and TDP fuel-to-water and fuel-to-electricity conversion factors α_h and β_h .

Proof. See the Appendix. \square

The diminishing marginal profit with g reflects the value of renewables in each region and mode. When the WDP is importing electricity (IM), additional renewables are valued at π^+ because they reduce grid purchases at π^+ . When the WDP is exporting electricity (EX), additional renewables are valued at π^- because they are sold to the grid at the export rate. In the off-grid region (NZ), additional renewables help in reducing (increasing) the reliance on TDP (RODP), and has dynamic values all of which are higher than π^- but lower than π^+ .

Lastly, the electricity payment and TDP operating costs monotonically decrease with renewables. The revenue from selling water is not monotonic.

V. NUMERICAL RESULTS

To showcase the optimal dispatch of the plant and the effect of tariff and plant parameters, we consider a WDP with TDP, RODP, and solar PV renewable generation. Semi-synthetic data is used in the simulation. In the base case, the plant faces a water utility that purchases desalinated water at a price $\pi^w = \$1/m^3$, and an electric utility that adopts an NEM X

tariff with a retail rate of $\pi^+ = \$270/\text{MWh}$ and a sell rate of $\pi^- = \$100/\text{MWh}$, respectively.

Typically, the TDP operating cost function is assumed to be convex quadratic $C_h(p_h) = ap_h^2 + bp_h + c$, with $a = \$0.008/\text{MBTU}^2$, $b = \$2/\text{MBTU}$, and $c = \$0$ [10]. The TDP and RODP flowrate limits were set as follows $\underline{w}_r = 8,333 \text{ m}^3/\text{h}$, $\bar{w}_h = 3,000 \text{ m}^3/\text{h}$, $\underline{w}_h = \bar{w}_h = 0 \text{ m}^3/\text{h}$. The conversion factors for TDP were set $\alpha_h = 4 \text{ m}^3/\text{MBTU}$, $\beta_h = 0.05 \text{ MWh}/\text{MBTU}$, $\eta_h = \alpha_h/\beta_h = 80 \text{ m}^3/\text{MWh}$. The conversion for RODP is $\alpha_r = 166.67 \text{ m}^3/\text{MWh}$.

We vary some of the technology and tariff parameters in the case study to evaluate their impact on WDP's optimal dispatch and profits. We used one-year hourly data obtained from Najran Province, Saudi Arabia, for a PV plant of assumed power capacity of 50 MW. The resulting average-day PV output profile is shown in Fig.4.

A. WDP Dispatch Algorithms

We compare the optimal WDP dispatch under the optimal joint dispatching of TDP, RODP, and renewables, in Theorem 1 and Proposition 2, to two other algorithms. To ensure a fair comparison, all modes have the same resources; additionally, they all face the same water and electricity tariffs.

1) *Max-RODP Algorithm:* In this case, the WDP sets the RODP to its maximum $w_r = \bar{w}_r$ and co-optimizes the renewables with the TDP; therefore, the optimal TDP dispatch becomes a special case of Theorem 1 and Proposition 2 with

$$w_h^*(g) = \begin{cases} w_h^{\text{IM}} & , g < \Gamma_{\text{IM}}^{\text{max}} \\ [\eta_h(\bar{w}_r/f'_r - g)]_{[\underline{w}_h, \bar{w}_h]} & , g \in [\Gamma_{\text{IM}}^{\text{max}}, \Gamma_{\text{EX}}^{\text{max}}] \\ w_h^{\text{EX}} & , g > \Gamma_{\text{EX}}^{\text{max}}, \end{cases} \quad (14)$$

where $\Gamma_{\sigma}^{\text{max}} = \bar{w}_r/f'_r - w_h^{\sigma}/\eta_h$, and w_h^{σ} is as in (7).

2) *Passive-TDP Dispatch Algorithm:* Here, the TDP is dispatched as if the plant was an independent water and power producer (IWPP), therefore the plant always faces π^- . As per corollary 2, the optimal TDP dispatch becomes $w_h^* = w_h^{\text{EX}}$, and as a result, from Theorem 1, $\Gamma_{\text{IM}} = \Gamma_{\text{NZ}_1}$ and $\Gamma_{\text{EX}} = \Gamma_{\text{NZ}_2}$. The optimal RODP is a two-threshold policy as in (9).

B. WDP Daily Dispatch

Figure 4 shows the WDP's optimal water output and net electricity consumption (top) and profits (bottom) under the three operating modes considered.

Under the optimal mode, the WDP remained self-sufficient throughout the day, so electricity revenue was always non-negative. During hours without solar generation, the RODP load was supplied entirely by the TDP, yielding about $2,583 \text{ m}^3$ (TDP) and $5,382 \text{ m}^3$ (RODP). As renewables increased, the plant allocated the additional energy to the RODP- whose marginal water value exceeded the value of exporting electricity-raising RODP output to $5,868 \text{ m}^3$ in hour 6 and $7,169 \text{ m}^3$ in hour 7. By hours 8-9, renewables drove the RODP to its maximum of $8,333 \text{ m}^3$, reducing reliance on the TDP.

Between hours 10 and 13, high renewable output pushed the WDP into net-export mode, forcing the TDP to its minimum ($1,750 \text{ m}^3$) because of the low export price π^- , while the

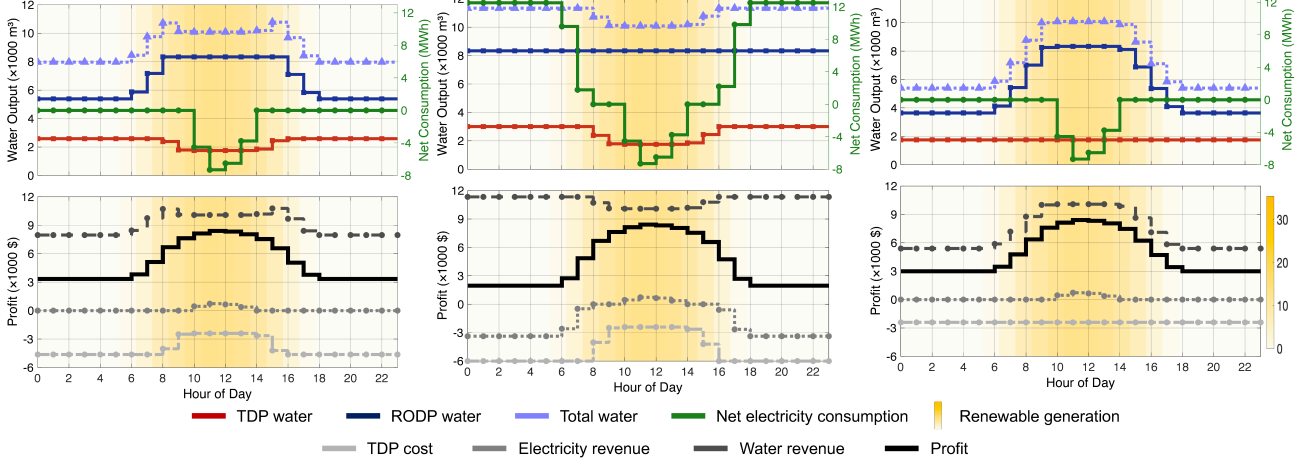


Fig. 4. WDP hourly dispatch and profits under the optimal joint dispatching (left), max-RODP algorithm (center), and passive-TDP algorithm (right).

RODP remained at maximum. A similar pattern repeated later in the day as solar output declined. Although electricity-export revenue was small, profits nearly tripled (from \$3,000 to \$8,400) due to higher water sales and lower TDP costs.

Under the *max-RODP* mode, only the TDP adjusted to renewable availability, causing the WDP to become a net electricity consumer during hours without solar generation. Profitability therefore declined, with profits near \$2,000 during these periods despite higher water-sales revenue.

In the *passive-TDP* mode, the TDP produced a fixed 1,750 m³/h, incurring a constant operating cost of \$2,406. Profits closely followed the water-revenue profile, as TDP costs were fixed and electricity-export revenue remained small because most renewables were consumed by the RODP. Total daily profits under *joint dispatching*, *max-RODP*, and *passive-TDP* were \$119,180, \$99,872, and \$112,850, respectively.

WDP Dispatch under low and high water prices: Figure 5 presents the hourly WDP dispatch and profits under the optimal dispatching algorithm for two water-price scenarios: a high price of $\pi^w = \$2/m^3$ (left panel) and a low price of $\pi^w = \$0.2/m^3$ (right panel). Under the high-price scenario, the RODP consistently operated at its maximum output of 8,333 m³. During hours without renewable generation, this output was supported by importing approximately 12 MWh from the grid, since the marginal revenue from water sales exceeds the marginal cost of electricity imports. The resulting total daily profit was \$366,320.

In contrast, when the water price was low, the RODP was off because exporting electricity is more profitable than producing additional water, effectively turning the facility into an IWPP. The TDP-based desalinated-water output remained constant at 950 m³/h, as the TDP operated at its minimum point while the plant was persistently in the net-export regime facing π^- . The total daily profit in this case dropped to \$36,372.

C. Sensitivity Analysis

Fig. 6 presents a profit sensitivity analysis with respect to the electricity tariff parameters (π^+ , π^-), the water tariff π^w , and the desalination technology parameters of the RO and TDP

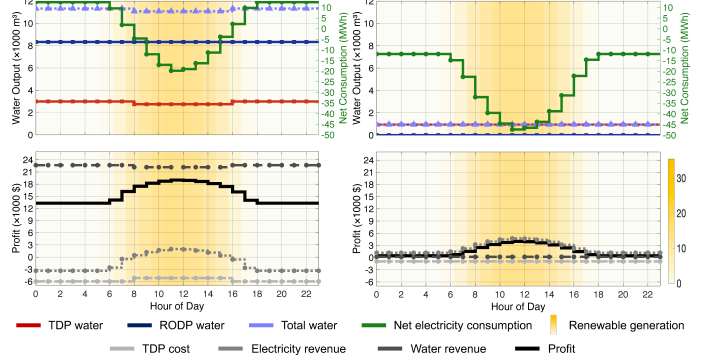


Fig. 5. WDP hourly dispatch and profits under the optimal policy, when $\pi^w = \$2/m^3$ (left) and $\pi^w = \$0.2/m^3$ (right).

units ($\alpha_r, \alpha_h, \beta_h$). For each sensitivity curve, all remaining parameters were fixed at the baseline values introduced at the beginning of this section.

Increasing the import price π^+ decreased the daily profit under all three control algorithms. For the optimal and passive-TDP schemes, however, this decline saturated once π^+ exceeded the threshold $\pi^+ = f'_r \pi^w \approx \$167/MWh$. Beyond this point, the RO desalination output collapsed to zero (see Proposition 2), and the WDP ceased to rely on grid electricity for RO dispatch, rendering the profit insensitive to further increases in π^+ .

Decreasing the export price π^- increased the profit monotonically for all algorithms. A kink appeared for the optimal and passive-TDP strategies near \$167/MWh, where the RO output reached its minimum, and the plant exported all locally generated power. Under the max-RODP algorithm, profit increased smoothly because electricity exports are valued at rising rates. Passive-TDP initially performed worse than max-RODP but surpassed it as the price gap $\Delta\pi$ narrowed, reducing the penalty associated with not adapting dynamically to the transition from π^+ to π^- .

The water price π^w exhibited the strongest influence on plant profitability. Under the optimal scheme, increasing π^w

from baseline to $\$2/m^3$ raised the profit by over 200%, with similar trends observed for max-RODP and passive-TDP.

The RO and TDP parameters also significantly impacted profitability. A higher TDP conversion factor β_h increased profits under all schemes, with particularly large gains for max-RODP because it relies heavily on TDP electricity when RO output is maximized to avoid costly grid imports.

Increasing the RO conversion factor α_r improved profits under all algorithms. Under max-RODP, profits grew from near zero at $\alpha_r = 125 m^3/MWh$ to nearly match the optimal algorithm at high α_r . When $\alpha_r \pi^w \geq \pi^+$, the optimal policy itself reduced to max-RODP dispatch.

Increasing the TDP conversion factor α_h consistently increased profits under the optimal and passive-TDP schemes, yielding about a 19% improvement relative to baseline. This is the only parameter regime in which passive-TDP uniformly outperformed max-RODP, since the latter benefits primarily from dynamically adjusting TDP output, an effect diminished when α_h dominated cost considerations. Under max-RODP, the effect of α_h was non-monotonic: profit first increased as additional water output and reduced electricity purchases outweighed fuel costs, but decreased beyond $\alpha_h \approx 5MWh/MBTU$ as increased TDP dispatch drove up grid imports.

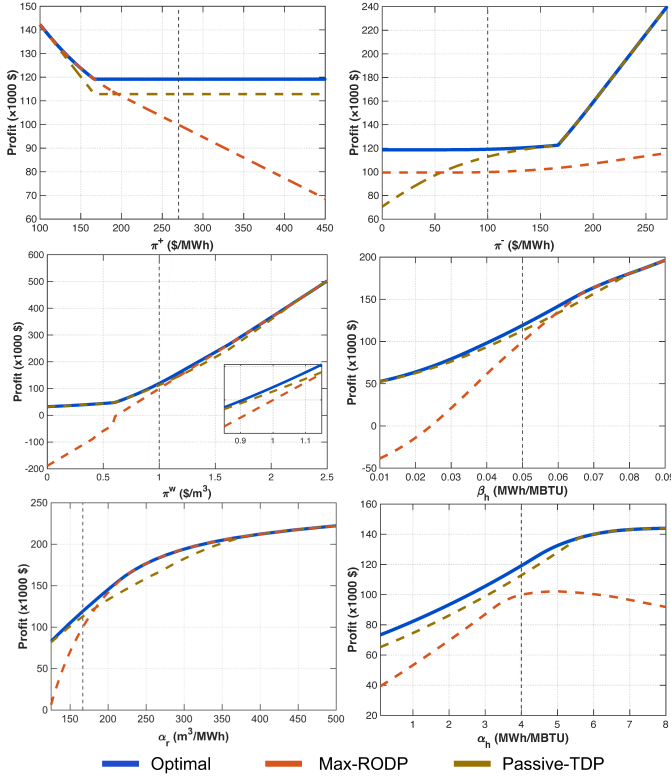


Fig. 6. Sensitivity of the WDP optimal daily profit and its suboptimal variants (max-RODP and passive-TDP) to π^+ , π^- , π^w , α_r , α_h , and β_h . The vertical dashed line indicates the baseline parameter value.

Sensitivity of Daily Profit to $\pm 50\%$ Variations in Tariff and Technology Parameters: Figure 7 decomposes the daily profit change under the optimal dispatching policy into TDP fuel cost, electricity revenue, and water revenue resulting from $\pm 50\%$ perturbations in the tariff and technology parameters.

used in Fig. 6. Each bar reports the contribution of each component, and the net impact Δ reflects the resulting profit change.

A 50% increase in the water price π^w produced the largest positive effect, raising daily profit by approximately $\$1.2M$ despite the higher TDP operating cost, because the increase in water-sales revenue dominated all other effects. Conversely, reducing π^w by 50% yields a profit loss of about $\$0.75M$: while TDP cost decreased (due to reduced TDP output) and electricity revenue increased (due to reduced RODP dispatch and thus lower imports), these gains were outweighed by the sharp decline in water-sales revenue.

Among the technology parameters, increasing the RO factor α_r by 50% yielded a pure-revenue gain of roughly $\$0.58M$, as higher RO efficiency increased water output without materially affecting TDP cost or electricity balance. Symmetrically, reducing α_r by 50% resulted in a comparable loss, driven entirely by reduced water-sales revenue.

Changes in the grid-import tariff π^+ have a negligible effect when increased by 50%, because the plant was never net-consuming over that range. A 50% decrease in π^+ produces only a modest profit increase (about $\$9.4k$); however, it reveals an interesting coupling between electricity and water dispatch in the WDP. Lower import prices incentivize increased RO dispatch, which in turn increases RO water output and electricity consumption, and thus raised water-sales revenue while increasing electricity costs. A similar coupling appears for the export price π^- : as π^- increased, exporting electricity became more profitable, increasing the incentive to run the TDP unit, which resulted in higher water-sales revenue and electricity revenue.

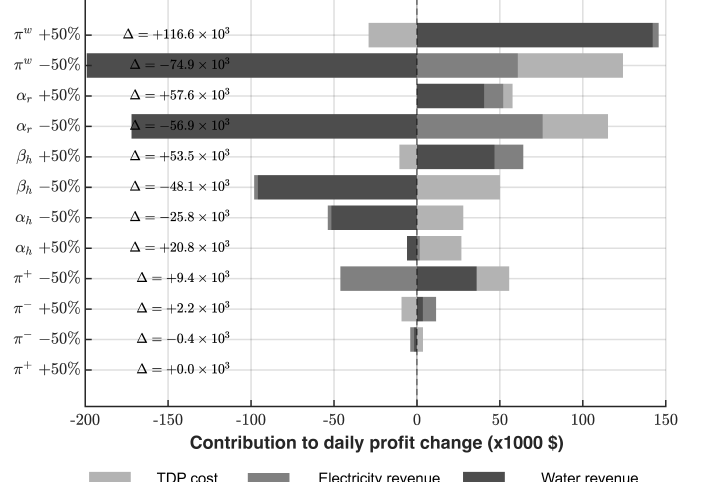


Fig. 7. Sensitivity of WDP daily profit to $\pm 50\%$ variations in tariff and technology parameters. The Δ represents the net daily profit change.

VI. CONCLUSION

We present a tractable analytical solution to the joint water-power dispatching problem for WDPs operating as hybrid generator-load resources, yielding valuable operational insights. The optimal dispatch exhibits a threshold-based structure determined solely by technology and tariff parameters,

and in some modes is independent of electricity prices. The coupled optimal dispatch of thermal and RO desalination is a function of local renewable generation, and is divided into five modes. When renewable generation is very low or very high, the WDP maintains fixed water production while using renewables to offset electricity imports or reduce exports. In the three intermediate modes, the WDP is net-zero, and the surplus renewables are allocated to water production: first by reducing thermal output, then by increasing RO output up to capacity, and finally by further displacing thermal generation when its marginal cost exceeds the export value of electricity.

The structural insights and performance benefits demonstrated through simulations showcase the potential to guide efficient dispatch of integrated water-energy systems in increasingly renewable-rich and market-responsive environments.

Several avenues for future research follow from the limitations of this work. First, incorporating energy storage would enable temporal shifting of desalinated water and electricity. Second, the model adopts rather simplified water-electricity conversion functions; in practice, energy-use depends on ambient conditions such as salinity and temperature. Third, our analysis focuses on short-run operations and abstracts from long-term investment decisions. Extending the framework to a joint planning-operation model would inform optimal sizing of desalination technologies and renewable capacity.

REFERENCES

- [1] A. S. Alahmed, A. Botterud, S. Amin, and A. T. Al-awami, "Watts and drops: Co-scheduling power and water in desalination plants," in *61st Annual Allerton Conference on Communication, Control, and Computing (Allerton)*, 2025. [Online]. Available: <https://hdl.handle.net/2142/126004>
- [2] K. Oikonomou and M. Parvania, "Optimal coordinated operation of interdependent power and water distribution systems," *IEEE Transactions on Smart Grid*, vol. 11, no. 6, pp. 4784–4794, 2020. doi: 10.1109/TSG.2020.3000173 .
- [3] A. Siddiqi and L. D. Anadon, "The water–energy nexus in middle east and north africa," *Energy Policy*, vol. 39, no. 8, pp. 4529–4540, 2011. doi: <https://doi.org/10.1016/j.enpol.2011.04.023> .
- [4] J. Eke, A. Yusuf, A. Giwa, and A. Sodiq, "The global status of desalination: An assessment of current desalination technologies, plants and capacity," *Desalination*, vol. 495, p. 114633, 2020. doi: <https://doi.org/10.1016/j.desal.2020.114633> .
- [5] Global Commission on the Economics of Water, "Turning the tide: A call to collective action," Global Commission on the Economics of Water, Tech. Rep., 03 2023. [Online]. Available: <https://watercommission.org/wp-content/uploads/2023/03/Turning-the-Tide-Report-Web.pdf>
- [6] M. Elimelech and W. A. Phillip, "The future of seawater desalination: Energy, technology, and the environment," *Science*, vol. 333, no. 6043, pp. 712–717, 2011. doi: 10.1126/science.1200488 .
- [7] N. Ghaffour, J. Bundschuh, H. Mahmoudi, and M. F. A. Goosen, "Renewable energy-driven desalination technologies: A comprehensive review on challenges and potential applications," *Desalination*, vol. 356, pp. 94–114, 2015. doi: 10.1016/j.desal.2014.10.024 .
- [8] R. O'Neil, K. Oikonomou, V. Tidwell, N. Voisin, J. Kerby, Z. Jason Hou, M. Parvania, A. T. Al-Awami, M. Panteli, S. A. Conrad, and T. K. A. Brekke, "Global research priorities for holistic integration of water and power systems," *IEEE Open Access Journal of Power and Energy*, vol. 11, pp. 457–468, 2024. doi: 10.1109/OAJPE.2024.3457448 .
- [9] P. H. Gleick, "Water and energy," *Annual Review of Environment and Resources*, vol. 19, no. Volume 19, 1994, pp. 267–299, 1994. doi: <https://doi.org/10.1146/annurev.e.19.110194.001411> .
- [10] A. Santhosh, A. M. Farid, and K. Youcef-Toumi, "Real-time economic dispatch for the supply side of the energy-water nexus," *Applied Energy*, vol. 122, pp. 42–52, 2014. doi: <https://doi.org/10.1016/j.apenergy.2014.01.062> .
- [11] A. M. Ghaithan, A. Mohammed, A. Al-Hanbali, A. M. Attia, and H. Saleh, "Multi-objective optimization of a photovoltaic-wind-grid connected system to power reverse osmosis desalination plant," *Energy*, vol. 251, p. 123888, 2022. doi: <https://doi.org/10.1016/j.energy.2022.123888> .
- [12] A. Qudah, A. Almerbati, and E. M. Mokheimer, "Novel approach for optimizing wind-pv hybrid system for RO desalination using differential evolution algorithm," *Energy Conversion and Management*, vol. 300, p. 117949, 2024. doi: <https://doi.org/10.1016/j.enconman.2023.117949> .
- [13] A. A. Almehizia, H. M. K. Al-Masri, and M. Ehsani, "Integration of renewable energy sources by load shifting and utilizing value storage," *IEEE Transactions on Smart Grid*, vol. 10, no. 5, pp. 4974–4984, 2019. doi: 10.1109/TSG.2018.2871806 .
- [14] L. Guo, W. Liu, X. Li, Y. Liu, B. Jiao, W. Wang, C. Wang, and F. Li, "Energy management system for stand-alone wind-powered-desalination microgrid," *IEEE Transactions on Smart Grid*, vol. 7, no. 2, pp. 1079–1087, 2016. doi: 10.1109/TSG.2014.2377374 .
- [15] F. Moazeni, J. Khazaei, and J. P. P. Mendes, "Maximizing energy efficiency of islanded micro water-energy nexus using co-optimization of water demand and energy consumption," *Applied Energy*, vol. 266, p. 114863, 2020. doi: <https://doi.org/10.1016/j.apenergy.2020.114863> .
- [16] F. Moazeni, J. Khazaei, and A. Asrari, "Step towards energy-water smart microgrids: buildings thermal energy and water demand management embedded in economic dispatch," *IEEE Transactions on Smart Grid*, vol. 12, no. 5, pp. 3680–3691, 2021. doi: 10.1109/TSG.2021.3068053 .
- [17] M. Elsir, A. T. Al-Awami, M. A. Antar, K. Oikonomou, and M. Parvania, "Risk-based operation coordination of water desalination and renewable-rich power systems," *IEEE Transactions on Power Systems*, vol. 38, no. 2, pp. 1162–1175, 2023. doi: 10.1109/TPWRS.2022.3174565 .
- [18] F. Mohammadi, M. Sahraei-Ardakani, Y. M. Al-Abdullah, and G. T. Heydt, "Coordinated scheduling of power generation and water desalination units," *IEEE Transactions on Power Systems*, vol. 34, no. 5, pp. 3657–3666, 2019. doi: 10.1109/TPWRS.2019.2901807 .
- [19] P. Zhao, S. Li, P. J.-H. Hu, C. Gu, S. Lu, S. Ding, Z. Cao, D. Xie, and Y. Xiang, "Blockchain-based water-energy transactive management with spatial-temporal uncertainties," *IEEE Transactions on Smart Grid*, vol. 14, no. 4, pp. 2903–2920, 2023. doi: 10.1109/TSG.2022.3230693 .
- [20] Y. Cao, B. Zhou, C. Y. Chung, Z. Shuai, Z. Hua, and Y. Sun, "Dynamic modelling and mutual coordination of electricity and watershed networks for spatio-temporal operational flexibility enhancement under rainy climates," *IEEE Transactions on Smart Grid*, vol. 14, no. 5, pp. 3450–3464, 2023. doi: 10.1109/TSG.2022.3223877 .
- [21] A. S. Zamzam, E. Dall'Anese, C. Zhao, J. A. Taylor, and N. D. Sidiropoulos, "Optimal water–power flow-problem: Formulation and distributed optimal solution," *IEEE Transactions on Control of Network Systems*, vol. 6, no. 1, pp. 37–47, 2019. doi: 10.1109/TCNS.2018.2792699 .
- [22] W. Gu and R. Sioshansi, "Enhanced convex relaxation approach for co-operated power and water systems," in *2025 IEEE Power Energy Society General Meeting (PESGM)*, 2025, pp. 1–5. doi: 10.1109/PESGM52009.2025.11225819 .
- [23] D. Koraki and K. Strunz, "Wind and solar power integration in electricity markets and distribution networks through service-centric virtual power plants," *IEEE Transactions on Power Systems*, vol. 33, no. 1, pp. 473–485, 2018. doi: 10.1109/TPWRS.2017.2710481 .
- [24] Q. Jiang, M. Xue, and G. Geng, "Energy management of microgrid in grid-connected and stand-alone modes," *IEEE Transactions on Power Systems*, vol. 28, no. 3, pp. 3380–3389, 2013. doi: 10.1109/TPWRS.2013.2244104 .
- [25] M. Al-Nory and M. El-Beltagy, "An energy management approach for renewable energy integration with power generation and water desalination," *Renewable Energy*, vol. 72, pp. 377–385, 2014. doi: <https://doi.org/10.1016/j.renene.2014.07.032> .
- [26] M. Mulder, *Basic Principles of Membrane Technology*. Springer Netherlands, 1996. doi: <https://doi.org/10.1007/978-94-009-1766-8> .
- [27] C. Sweeney, R. J. Bessa, J. Browell, and P. Pinson, "The future of forecasting for renewable energy," *WIREs Energy and Environment*, vol. 9, no. 2, p. e365, 2020. doi: <https://doi.org/10.1002/wene.365> .
- [28] Y. Chen, Y. Wang, D. Kirschen, and B. Zhang, "Model-free renewable scenario generation using generative adversarial networks," *IEEE Transactions on Power Systems*, vol. 33, no. 3, pp. 3265–3275, 2018. doi: 10.1109/TPWRS.2018.2794541 .
- [29] A. S. Alahmed and L. Tong, "On net energy metering X: Optimal prosumer decisions, social welfare, and cross-subsidies," *IEEE Transactions on Smart Grid*, vol. 14, no. 02, 2023. doi: 10.1109/TSG.2022.3158951 .
- [30] S. Boyd and L. Vandenberghe, *Convex Optimization*. Cambridge University Press, 2004. doi: <https://doi.org/10.1017/CBO9780511804441> .

A. Proof of Lemma 1

The first term in the profit function in (4), $R^w(w_h, w_r)$, is affine, hence concave. Also, the second term is a piecewise linear concave function, because by re-expressing it as

$$P(z(\frac{w_h}{\eta_h}, \frac{w_r}{\alpha_r})) = \max \left(\pi^+ z(\frac{w_h}{\eta_h}, \frac{w_r}{\alpha_r}), \pi^- z(\frac{w_h}{\eta_h}, \frac{w_r}{\alpha_r}) \right),$$

and given $\pi^+ \geq \pi^-$, one can see that it is the pointwise maximum of two affine functions, which is convex [30]. Lastly the third term $-C_h(w_h/\alpha_h)$ is strictly concave in w_h , since, by assumption, $C_h(\cdot)$ is strictly convex. Therefore, the profit is concave in w_r , as the sum of concave functions is concave. The profit is strictly concave in w_h because the sum of concave and strictly concave functions is strictly concave [30]. \square

B. Proof of Theorem 1

We equivalently re-write the problem to the following

$$\begin{aligned} \min_{q_r, q_h, w_r, w_h} \quad & -\pi^w(w_r + w_h) + \pi^+[z(q_r, q_h)]^+ - \pi^-[z(q_r, q_h)]^- \\ & + C_h(p_h) \\ \text{s.t.} \quad & z = q_r - q_h - g, \\ & \underline{w}_r \leq \alpha_r q_r \leq \bar{w}_r, \\ & \underline{w}_h \leq \eta_h q_h \leq \bar{w}_h, \end{aligned}$$

and note that $w_r = \alpha_r, w_h = \eta_h q_h$.

We divide the problem above into three convex and differentiable sub-problems based on z as: $\mathcal{P}^{\text{IM}} : z > 0, \mathcal{P}^{\text{EX}} : z < 0, \mathcal{P}^{\text{NZ}} : z = 0$.

Since Slater's condition holds for these optimization problems, the KKT conditions are both necessary and sufficient for optimality.

Solution to \mathcal{P}^{IM} : Under \mathcal{P}^{IM} , the problem becomes

$$\begin{aligned} \min_{q_r, q_h} \quad & -\pi^w(\alpha_r q_r + \eta_h q_h) + \pi^+(q_r - q_h - g) + C_h(p_h(q_h)) \\ \text{s.t.} \quad & q_r - q_h - g \geq 0, \\ & \underline{w}_r \leq \alpha_r q_r \leq \bar{w}_r, \\ & \underline{w}_h \leq \eta_h q_h \leq \bar{w}_h \end{aligned}$$

The Lagrangian is:

$$\begin{aligned} \mathcal{L}^{\text{IM}} = & -\pi^w(\alpha_r q_r + \eta_h q_h) + (\pi^+ - \mu^{\text{IM}})(q_r - q_h - g) \\ & + C_h(p_h) + \underline{\lambda}_r^{\text{IM}}(\underline{w}_r - \alpha_r q_r) + \bar{\lambda}_r^{\text{IM}}(\alpha_r q_r - \bar{w}_r) \\ & + \underline{\lambda}_h^{\text{IM}}(\underline{w}_h - \eta_h q_h) + \bar{\lambda}_h^{\text{IM}}(\eta_h q_h - \bar{w}_h), \end{aligned}$$

with $\mu^{\text{IM}} = 0$ because $z \geq 0$ is explicitly enforced here and the active case $\mu > 0$ is handled in \mathcal{P}^{NZ} . $\underline{\lambda}_r^{\text{IM}}, \bar{\lambda}_r^{\text{IM}}, \underline{\lambda}_h^{\text{IM}}, \bar{\lambda}_h^{\text{IM}} \geq 0$ are the Lagrange multipliers of the RO and thermal minimum and maximum water output limits,

Note that the objective is linear w.r.t. q_r , over a convex set, and we are given $f'_r \pi^w \leq \pi^+$, hence the optimal solution is $q_r^{\text{IM}} = \underline{w}_r/\alpha_r$, which yields, using the conversion function, $w_r^{\text{IM}} = \underline{w}_r$.

Stationarity in q_h gives

$$\frac{\partial \mathcal{L}^{\text{IM}}}{\partial q_h^{\text{IM}}} = -\eta_h \pi^w - \pi^+ + \frac{\eta_h}{\alpha_h} C'_h(p_h) - \eta_h \underline{\lambda}_h^{\text{IM}} + \eta_h \bar{\lambda}_h^{\text{IM}} = 0,$$

leading to

$$q_h^{\text{IM}} = \max \left\{ \frac{\underline{w}_h}{\eta_h}, \min \left\{ \frac{\alpha_h}{\eta_h} D_h(\alpha_h \pi^w + \beta_h \pi^+), \frac{\bar{w}_h}{\eta_h} \right\} \right\},$$

and $w_h^{\text{IM}} := \eta_h q_h^{\text{IM}}$. The solution is feasible only if the resulting

$$z^{\text{IM}}(g) = q_r^{\text{IM}} - q_h^{\text{IM}} - g > 0,$$

which holds for all $g < q_r^{\text{IM}} - q_h^{\text{IM}} =: \Gamma_{\text{IM}}$, under which

$$w_h^{\text{IM}} = \max \{ \underline{w}_h, \min \{ \alpha_h D_h(\alpha_h \pi^w + \beta_h \pi^+), \bar{w}_h \} \}.$$

Solution to \mathcal{P}^{EX} : Under \mathcal{P}^{EX} , the problem becomes

$$\begin{aligned} \min_{q_r, q_h} \quad & -\pi^w(\alpha_r q_r + \eta_h q_h) + \pi^-(q_r - q_h - g) + C_h(p_h(q_h)) \\ \text{s.t.} \quad & q_r - q_h - g \leq 0, \\ & \underline{w}_r \leq \alpha_r q_r \leq \bar{w}_r, \\ & \underline{w}_h \leq \eta_h q_h \leq \bar{w}_h \end{aligned}$$

By symmetry to the \mathcal{P}^{IM} problem, we obtain the optimal solutions $w_r^{\text{EX}} = \bar{w}_r$, and

$$w_h^{\text{EX}} = \max \{ \underline{w}_h, \min \{ \alpha_h D_h(\alpha_h \pi^w + \beta_h \pi^-), \bar{w}_h \} \}.$$

Using the conversion functions, we have $q_r^{\text{EX}} = w_r^{\text{EX}}/\alpha_r$ and $q_h^{\text{EX}} = w_h^{\text{EX}}/\eta_h$.

Feasibility of the export region requires

$$z^{\text{EX}}(g) = q_r^{\text{EX}} - q_h^{\text{EX}} - g < 0,$$

which holds for all $g > q_r^{\text{EX}} - q_h^{\text{EX}} =: \Gamma_{\text{EX}}$

Solution to \mathcal{P}^{NZ} : Under \mathcal{P}^{NZ} , the problem becomes

$$\begin{aligned} \min_{q_r, q_h} \quad & -\pi^w(\alpha_r q_r + \eta_h q_h) + C_h(p_h) \\ \text{s.t.} \quad & q_r - q_h - g = 0, \\ & \underline{w}_r \leq \alpha_r q_r \leq \bar{w}_r, \\ & \underline{w}_h \leq \eta_h q_h \leq \bar{w}_h \end{aligned}$$

The net-zero region enforces the equality

$$q_r - q_h - g = 0, \quad (15)$$

which is imposed with multiplier μ^{NZ} . The Lagrangian for the NZ region reads

$$\begin{aligned} \mathcal{L}^{\text{NZ}} = & -\pi^w(\alpha_r q_r + \eta_h q_h) + C_h(p_h) + \mu^{\text{NZ}}(q_r - q_h - g) \\ & + \underline{\lambda}_r^{\text{NZ}}(\underline{w}_r - \alpha_r q_r) + \bar{\lambda}_r^{\text{NZ}}(\alpha_r q_r - \bar{w}_r) \\ & + \underline{\lambda}_h^{\text{NZ}}(\underline{w}_h - \eta_h q_h) + \bar{\lambda}_h^{\text{NZ}}(\eta_h q_h - \bar{w}_h), \end{aligned}$$

with $\underline{\lambda}_r^{\text{NZ}}, \bar{\lambda}_r^{\text{NZ}}, \underline{\lambda}_h^{\text{NZ}}, \bar{\lambda}_h^{\text{NZ}} \geq 0$.

a) Stationarity conditions.: Differentiating w.r.t. q_r and q_h and using $\partial p_h / \partial q_h = 1/\beta_h$ (from $w_h = \alpha_h p_h = \eta_h q_h$) yields

$$0 = -\alpha_r \pi^w + \mu^{\text{NZ}} - \alpha_r \underline{\lambda}_r^{\text{NZ}} + \alpha_r \bar{\lambda}_r^{\text{NZ}}, \quad (16)$$

$$0 = -\eta_h \pi^w - \mu^{\text{NZ}} + \frac{\eta_h}{\alpha_h} C'_h(p_h) - \eta_h \underline{\lambda}_h^{\text{NZ}} + \eta_h \bar{\lambda}_h^{\text{NZ}}. \quad (17)$$

Rearranging (16)–(17) gives the standard pair

$$\mu^{\text{NZ}} = \alpha_r(\pi^w + \underline{\lambda}_r^{\text{NZ}} - \bar{\lambda}_r^{\text{NZ}}), \quad (18)$$

$$\mu^{\text{NZ}} = \eta_h \left(-\pi^w + \frac{1}{\alpha_h} C'_h(p_h) - \underline{\lambda}_h^{\text{NZ}} + \bar{\lambda}_h^{\text{NZ}} \right). \quad (19)$$

Interior NZ solution (no bounds active): If none of the bound multipliers are active $\underline{\lambda}_r^{\text{NZ}} = \bar{\lambda}_r^{\text{NZ}} = \underline{\lambda}_h^{\text{NZ}} = \bar{\lambda}_h^{\text{NZ}} = 0$, equating (18) and (19) yields

$$\alpha_r \pi^w = \eta_h \left(-\pi^w + \frac{1}{\alpha_h} C'_h(p_h) \right).$$

Solving for $C'_h(p_h)$ and applying $p_h = D_h(\cdot)$ gives

$$p_h^{\text{NZ,int}} = D_h \left(\alpha_h \left(\pi^w \left(1 + \frac{\alpha_r}{\eta_h} \right) \right) \right),$$

which yields

$$q_h^{\text{NZ,int}} = \beta_h D_h \left(\alpha_h \pi^w + \beta_h \alpha_r \pi^w \right) = q_h^* \quad (20)$$

Then the NZ equality (15) gives

$$q_r^{\text{NZ,int}} = q_h^{\text{NZ,int}} + g. \quad (21)$$

Consequently

$$w_h^{\text{NZ,int}} = \eta_h q_h^{\text{NZ,int}}, \quad w_r^{\text{NZ,int}} = \alpha_r (q_h^{\text{NZ,int}} + g). \quad (22)$$

The interior NZ solution is feasible only if both

$$\underline{w}_h \leq \eta_h q_h^{\text{NZ,int}} \leq \bar{w}_h, \quad \underline{w}_r \leq \alpha_r (q_h^{\text{NZ,int}} + g) \leq \bar{w}_r. \quad (23)$$

The first condition in (23) depends only on parameters; if it fails the interior solution is impossible for every g . Solving the second condition for g yields the RODP-derived interval

$$\frac{\underline{w}_r}{\alpha_r} - q_h^* \leq g \leq \frac{\bar{w}_r}{\alpha_r} - q_h^*.$$

Accordingly define

$$\Gamma_{\text{NZ}_1} := \frac{\underline{w}_r}{\alpha_r} - q_h^*, \quad \Gamma_{\text{NZ}_2} := \frac{\bar{w}_r}{\alpha_r} - q_h^*. \quad (24)$$

Thus, if the TDP bound $\underline{w}_h \leq \eta_h q_h^* \leq \bar{w}_h$ holds, the interior NZ solution is feasible exactly for

$$g \in [\Gamma_{\text{NZ}_1}, \Gamma_{\text{NZ}_2}].$$

If the TDP bound does not hold, the interior NZ solution is infeasible for all g , and the NZ optimum must be a boundary solution for every g .

We now characterize which boundary (RODP or TDP, lower or upper) is active depending on g . There are two cases.

Case A: TDP bounds satisfied for the interior candidate.

Assume

$$\underline{w}_h \leq \eta_h q_h^* \leq \bar{w}_h.$$

Then the interior NZ solution is feasible for $g \in [\Gamma_{\text{NZ}_1}, \Gamma_{\text{NZ}_2}]$. For g outside this interval the interior candidate violates the RODP bounds and the NZ optimum lies on the corresponding RODP boundary:

• $g < \Gamma_{\text{NZ}_1}$ (RODP lower-bound violation): The interior candidate requires $\alpha_r (q_h^* + g) < \underline{w}_r$. Enforcing the RODP lower bound yields the RODP lower-boundary NZ solution

$$q_r = \frac{\underline{w}_r}{\alpha_r}, \quad q_h = \frac{\underline{w}_r}{\alpha_r} - g,$$

so the NZ pair is

$$w_r^{\text{NZ,lb}} = \underline{w}_r, \quad w_h^{\text{NZ,lb}}(g) = \eta_h \left(\frac{\underline{w}_r}{\alpha_r} - g \right).$$

This solution is valid provided the computed $w_h^{\text{NZ,lb}}(g)$ respects the TDP bounds: $\underline{w}_h \leq w_h^{\text{NZ,lb}}(g) \leq \bar{w}_h$. If it violates TDP bounds then the (TDP) bound will be active as described in Case B below.

• $g > \Gamma_{\text{NZ}_2}$ (RODP upper-bound violation): The interior candidate requires $\alpha_r (q_h^* + g) > \bar{w}_r$. Enforcing the RODP upper bound yields the RODP upper-boundary NZ solution

$$q_r = \frac{\bar{w}_r}{\alpha_r}, \quad q_h = \frac{\bar{w}_r}{\alpha_r} - g,$$

so the NZ pair is

$$w_r^{\text{NZ,ub}} = \bar{w}_r, \quad w_h^{\text{NZ,ub}}(g) = \eta_h \left(\frac{\bar{w}_r}{\alpha_r} - g \right),$$

valid provided $\underline{w}_h \leq w_h^{\text{NZ,ub}}(g) \leq \bar{w}_h$. If this TDP check fails then revert to Case B behavior.

Case B: TDP bounds violated by the interior candidate. If either $\eta_h q_h^* < \underline{w}_h$ or $\eta_h q_h^* > \bar{w}_h$, then the interior NZ candidate is infeasible for all g . In this situation the NZ optimal solution must make w_h equal the violated TDP bound, and the NZ equality (15) then pins q_r . Concretely:

• $\eta_h q_h^* < \underline{w}_h$: the TDP lower bound is mandatory. Set $q_h = \underline{w}_h / \eta_h$ and enforce $q_r = q_h + g$. The NZ pair is

$$w_h^{\text{NZ}} = \underline{w}_h, \quad w_r^{\text{NZ}}(g) = \alpha_r \left(\frac{\underline{w}_h}{\eta_h} + g \right).$$

Verify whether $w_r^{\text{NZ}}(g)$ respects RODP bounds; if it violates RODP bounds then the solution projects to the intersection of active bounds (e.g., both lower bounds).

• $\eta_h q_h^* > \bar{w}_h$: the TDP upper bound is mandatory. Set $q_h = \bar{w}_h / \eta_h$ and enforce $q_r = q_h + g$. The NZ pair is

$$w_h^{\text{NZ}} = \bar{w}_h, \quad w_r^{\text{NZ}}(g) = \alpha_r \left(\frac{\bar{w}_h}{\eta_h} + g \right).$$

Again check RODP feasibility and project onto active intersections if needed.

Selection of the Optimal Region.

Let the IM and EX KKT solutions yield feasible pairs $(q_r^{\text{IM}}, q_h^{\text{IM}})$ and $(q_r^{\text{EX}}, q_h^{\text{EX}})$, and define

$$\Gamma_{\text{IM}} := q_r^{\text{IM}} - q_h^{\text{IM}}, \quad \Gamma_{\text{EX}} := q_r^{\text{EX}} - q_h^{\text{EX}}.$$

Let the interior NZ solution (20)–(21) be feasible for $g \in [\Gamma_{\text{NZ}_1}, \Gamma_{\text{NZ}_2}]$. Each region (IM, NZ, EX) corresponds to a convex restriction of the original problem to a fixed sign of $z = q_r - q_h - g$. By convexity and Slater's condition, the region-wise KKT point is globally optimal within its region. Hence the global optimizer is the region-consistent KKT solution.

The optimal regime as a function of g is therefore

$$\begin{cases} \text{IM}, & g < \Gamma_{\text{IM}}, \\ \text{NZ-lower boundary}, & \Gamma_{\text{IM}} \leq g \leq \Gamma_{\text{NZ}_1}, \\ \text{NZ-interior}, & \Gamma_{\text{NZ}_1} \leq g \leq \Gamma_{\text{NZ}_2}, \\ \text{NZ-upper boundary}, & \Gamma_{\text{NZ}_2} \leq g \leq \Gamma_{\text{EX}}, \\ \text{EX}, & g > \Gamma_{\text{EX}}. \end{cases}$$

b) *Remark (Equality cases).*: The derivation above assumed strict inequalities between $f'_r \pi^w$ and the boundary prices π^+, π^- . We now treat the two equality cases, which correspond to indifference of the objective to small variations of the RODP decision and hence to possible non-uniqueness of the RODP optimum.

(i) $f'_r \pi^w = \pi^+$. From the stationarity condition for the IM problem the objective is flat in q_r at interior points, so the complementary slackness conditions allow either an interior q_r or an active RODP upper bound. In particular, both the IM-region boundary solution $w_r = \bar{w}_r$ and any w_r in the feasible interval that satisfies the remaining KKT conditions are optimal. Equivalently, the limiting behaviour under an arbitrarily small increase of π^+ (so that $f'_r \pi^w > \pi^+$) selects $w_r = \bar{w}_r$; under an arbitrarily small decrease of π^+ the lower boundary becomes preferred. Thus the set of optimal RODP outputs at equality is the convex set of KKT-feasible w_r .

(ii) $f'_r \pi^w = \pi^-$. A symmetric statement holds: the EX-region stationarity is flat in q_r at equality and both $w_r = \underline{w}_r$ and any KKT-feasible interior value are optimal; the limit under perturbations of π^- breaks the tie.

□

C. Proof of Corollary 1

The corollary follows directly from the monotonicity of the cost function $C_h(\cdot)$, the conversion function $f_h(\cdot)$, the ratio η_h , and the assumption $f'_r \pi^w \in [\pi^-, \pi^+]$, which yield $w_h^{\text{IM}} \geq w_h^{\text{NZ}} \geq w_h^{\text{EX}}$, and $\bar{w}_r \geq \underline{w}_r$, therefore

$$\begin{aligned} \Gamma_{\text{EX}} &:= \bar{w}_r / f'_r - w_h^{\text{EX}} / \eta_h \\ &\geq \bar{w}_r / f'_r - w_h^{\text{NZ}} / \eta_h =: \Gamma_{\text{NZ}} \\ &\geq \underline{w}_r / f'_r - w_h^{\text{NZ}} / \eta_h =: \Gamma_{\text{NZ}_1} \\ &\geq \underline{w}_r / f'_r - w_h^{\text{IM}} / \eta_h =: \Gamma_{\text{IM}}. \end{aligned}$$

The monotonic threshold-difference ($\Gamma_{\text{EX}} - \Gamma_{\text{IM}}$) increases with $\Delta\pi$ can be easily shown from the inequality above. □

D. Proof of Proposition 1

By definition,

$$z^*(g) = q_r^* - q_h^* - g = w_r^* / \alpha_r - w_h^* / \eta_h - g.$$

From (8)-(9) in Theorem 1, we can write $z^*(g)$ as

$$z^*(g) = \begin{cases} \underline{w}_r / f'_r - w_h^{\text{IM}} / \eta_h - g & , g < \Gamma_{\text{IM}} \\ 0 & , g \in [\Gamma_{\text{IM}}, \Gamma_{\text{EX}}] \\ \bar{w}_r / f'_r - w_h^{\text{EX}} / \eta_h - g & , g > \Gamma_{\text{EX}}, \end{cases} \quad (25)$$

where the middle segment is zero since, over the intervals ($g \in [\Gamma_{\text{IM}}, \Gamma_{\text{NZ}_1}]$) and ($g \in (\Gamma_{\text{NZ}_2}, \Gamma_{\text{EX}}]$), we have $(f'_h w_h^*(g) = f'_r w_r^* - g)$, which implies $(z^*(g) = 0)$. And when $g \in [\Gamma_{\text{NZ}_1}, \Gamma_{\text{NZ}_2}]$,

$$z^*(g) = f'_h w_h^{\text{NZ}} + g - f'_r w_h^{\text{NZ}} - g = 0.$$

From the threshold expressions in (6), and the conditions in (25), we conclude that the first piece in (25) is positive, the second is zero, and the third is negative. □

E. Proof of Proposition 2

Assume $f'_r \pi^w \notin [\pi^-, \pi^+]$. There are two mutually exclusive cases.

Case A: $f'_r \pi^w > \pi^+$. By Theorem 1 (and its IM/EX solutions) the RODP optimal choice in the IM region is

$$w_r^{\text{IM}} = \bar{w}_r \quad \text{iff} \quad f'_r \pi^w > \pi^+,$$

and in the EX region

$$w_r^{\text{EX}} = \bar{w}_r \quad \text{iff} \quad f'_r \pi^w > \pi^-.$$

Since $\pi^+ \geq \pi^-$, $f'_r \pi^w > \pi^+$ implies $f'_r \pi^w > \pi^-$ and therefore $w_r^{\text{IM}} = w_r^{\text{EX}} = \bar{w}_r$. By continuity of the KKT solutions across regions (Theorem 1 proof) the same \bar{w}_r is optimal for all three regions (IM, NZ, EX); hence $w_r^* = \bar{w}_r$ for all g .

Case B: $f'_r \pi^w < \pi^-$. Analogous reasoning using Theorem 1 gives $w_r^{\text{IM}} = w_r^{\text{EX}} = \underline{w}_r$, and thus $w_r^* = \underline{w}_r$ for all g .

Thus under the stated assumption the RODP optimal output is constant in g and equal to the appropriate boundary:

$$w_r^* = \begin{cases} \bar{w}_r, & f'_r \pi^w > \pi^+, \\ \underline{w}_r, & f'_r \pi^w < \pi^-. \end{cases}$$

(When $\pi^+ = \pi^-$ the same formula applies with the two inequalities coinciding.)

Having established that w_r^* is fixed at a bound (independent of g) in the special-tariff cases, the TDP decision reduces to a single-variable optimization version of (5) with fixed w_r^* and q_r^* . Such optimization give rise to a two-threshold policy partitioning the range of g into three zones as shown in [29]. As a result, given the two thresholds

$$\Gamma_{\text{IM}}^s := \frac{w_r^*}{f'_r} - \frac{w_h^{\text{IM}}}{\eta_h}, \quad \Gamma_{\text{EX}}^s := \frac{w_r^*}{f'_r} - \frac{w_h^{\text{EX}}}{\eta_h},$$

with the TDP optimal outputs, w_h^{IM} and w_h^{EX} , computed in Theorem 1 under the IM and EX price terms, the optimal TDP output is

$$w_h^*(g) = \begin{cases} w_h^{\text{IM}}, & g < \Gamma_{\text{IM}}^s, \\ \left[\eta_h \left(\frac{w_r^*}{f'_r} - g \right) \right]_{[\underline{w}_r, \bar{w}_r]}, & \Gamma_{\text{IM}}^s \leq g \leq \Gamma_{\text{EX}}^s, \\ w_h^{\text{EX}}, & g > \Gamma_{\text{EX}}^s, \end{cases}$$

Finally, when $\pi^+ = \pi^-$ the IM and EX price terms coincide and one obtains $w_h^{\text{IM}} = w_h^{\text{EX}} = w_h^*$, recovering the degenerate single-threshold (or constant) case described in the proposition. □

F. Proof of Corollary 2

The proof follows directly from Theorem 1. In the RODP-only case, all TDP inputs are zeroed, and from (6), this yields $\Gamma_{\text{IM}} = \Gamma_{\text{NZ}_1} = \underline{w}_r / f'_r$ and $\Gamma_{\text{EX}} = \Gamma_{\text{NZ}_2} = \bar{w}_r / f'_r$. For which (9) becomes equivalent to (13).

In the TDP-only case, all thresholds in (6) become negative, and because $g > \Gamma_{\text{EX}}$, the WDP is always in the net-production region; hence, from (8), we have $w_h^* = w_h^{\text{EX}}$. □

G. Proof of Theorem 2

Define the maximized profit under Theorem 1 controls as

$$\Pi^*(g) := \Pi(w_h^*(g), w_r^*(g), q_h^*(g), q_r^*(g); g),$$

with $q_h^* = w_h^*/\eta_h$, $q_r^* = w_r^*/f'_r$, and $z^* := q_r^* - q_h^* - g$. We compute $\frac{d\Pi^*}{dg}$ by substituting the region-specific expressions for $(w_h^*, w_r^*, q_h^*, q_r^*)$ from Theorem 1 and differentiating.

– $g < \Gamma_{\text{IM}}$ (**IM**). From Theorem 1 we have $w_h^* = w_h^{\text{IM}}$ and $w_r^* = \underline{w}_r$. Differentiating the profit yields

$$\frac{d\Pi^*}{dg} = -\pi^+(-1) = \pi^+.$$

Hence in the IM region the maximized profit increases with g at rate π^+ .

– $g \in [\Gamma_{\text{IM}}, \Gamma_{\text{NZ}_1}]$ (**NZ**) From Theorem 1 we have

$$w_r^*(g) = \underline{w}_r, \quad w_h^*(g) = \eta_h \left(\frac{\underline{w}_r}{f'_r} - g \right),$$

so

$$q_r^* = \frac{\underline{w}_r}{f'_r}, \quad q_h^* = \frac{w_h^*}{\eta_h} = \frac{\underline{w}_r}{f'_r} - g,$$

and therefore $z^* = q_r^* - q_h^* - g = 0$, and the profit becomes

$$\Pi^*(g) = \pi^w (w_h^* + \underline{w}_r) - C_h(p_h^*),$$

which when differentiated gives

$$\frac{d\Pi^*}{dg} = \pi^w \frac{dw_h^*}{dg} - C'_h(p_h^*) \frac{dp_h^*}{dg}. \quad (26)$$

Since $w_h^* = \eta_h(\underline{w}_r/f'_r - g)$ we have $dw_h^*/dg = -\eta_h$, and $p_h^* = w_h^*/\alpha_h$ so $dp_h^*/dg = -\eta_h/\alpha_h$. Substituting into (26) gives

$$\frac{d\Pi^*}{dg} = -\eta_h \pi^w + \frac{\eta_h}{\alpha_h} C'_h(p_h^*).$$

Next use the stationarity (first-order) condition for the TDP at the optimal point. Writing the Lagrangian of the inner maximization (and denoting by μ^{NZ} the multiplier associated with the power balance) yields the p_h -stationarity

$$\alpha_h \pi^w - C'_h(p_h^*) - \beta_h \mu^{\text{NZ}} = 0,$$

hence

$$C'_h(p_h^*) = \alpha_h \pi^w - \beta_h \mu^{\text{NZ}}.$$

Substitute this into the expression for $d\Pi^*/dg$ to obtain

$$\frac{d\Pi^*}{dg} = -\eta_h \pi^w + \frac{\eta_h}{\alpha_h} (\alpha_h \pi^w - \beta_h \mu^{\text{NZ}}) = -\eta_h \frac{\beta_h}{\alpha_h} \mu^{\text{NZ}}.$$

Using $\beta_h/\alpha_h = 1/\eta_h$ (since $w_h = \alpha_h p_h = \eta_h q_h$ and $\beta_h q_h = p_h$) the prefactors cancel and we obtain the clean identity

$$\frac{d\Pi^*}{dg} = \mu^{\text{NZ}}.$$

Thus the slope equals the electricity-balance multiplier μ^{NZ} in this net-zero region.

It remains to bound μ^{NZ} . Examining the neighbouring regions shows that the two adjacent marginal values are π^+ (IM side) and the NZ marginal value $f'_r \pi^w$ (NZ interior). Therefore the KKT/subgradient conditions imply

$$\mu^{\text{NZ}} \in [\pi^+, f'_r \pi^w],$$

and combining with $\frac{d\Pi^*}{dg} = \mu^{\text{NZ}}$ yields $\frac{d\Pi^*}{dg} \in [\pi^+, f'_r \pi^w]$, as claimed.

– $g \in [\Gamma_{\text{NZ}_1}, \Gamma_{\text{NZ}_2}]$ (**NZ**). Theorem 1 gives

$$w_h^* = w_h^{\text{NZ}} \quad (\text{constant}), \quad w_r^* = f'_r \left(\frac{w_h^{\text{NZ}}}{\eta_h} + g \right).$$

Thus $q_r^* - q_h^* - g = 0$ for all g in this interval. Differentiating the profit directly yields

$$\frac{d\Pi^*}{dg} = \pi^w \frac{dw_r^*}{dg} = \pi^w f'_r.$$

Therefore, in this region, the maximized profit increases at $f'_r \pi^w$.

– $g \in (\Gamma_{\text{NZ}_2}, \Gamma_{\text{EX}}]$ (**NZ**). This interval is symmetric to Region B. Theorem 1 gives $w_r^* = \bar{w}_r$ and

$$w_h^*(g) = \eta_h \left(\frac{\bar{w}_r}{f'_r} - g \right),$$

hence, repeating the algebra from Region $g \in [\Gamma_{\text{IM}}, \Gamma_{\text{NZ}_1}]$ yields

$$\frac{d\Pi^*}{dg} = \mu^{\text{NZ}},$$

where now the multiplier μ^{NZ} is bounded between the NZ marginal value and the EX-side marginal value, *i.e.*,

$$\mu^{\text{NZ}} \in [f'_r \pi^w, \pi^-].$$

Therefore, $\frac{d\Pi^*}{dg} \in [f'_r \pi^w, \pi^-]$, as stated.

– $g > \Gamma_{\text{EX}}$ (**EX**). Theorem 1 Similar to IM region, differentiating the profit yields,

$$\frac{d\Pi^*}{dg} = -\frac{\partial P}{\partial z} \Big|_{z^*} \frac{dz^*}{dg} = -\pi^-(-1) = \pi^-.$$

Thus in EX the profit increases with g at rate π^- .

– **Monotonicity in prices and conversion factors.** By the envelope theorem, we have

$$\frac{\partial \Pi^*}{\partial \pi^+} = -[z^*]^+ \leq 0, \quad \frac{\partial \Pi^*}{\partial \pi^-} = -[z^*]^- \geq 0, \quad \frac{\partial \Pi^*}{\partial \pi^w} = w_h^* + w_r^* \geq 0.$$

Increasing conversion factors $\alpha_h, \beta_h, \alpha_r$ increases feasible water output per unit fuel/energy and therefore (since revenues grow while costs are convex in fuel) cannot decrease the maximized profit; hence the profit is nondecreasing in these parameters (and strictly increasing under mild interiority assumptions). \square